THE JOURNAL OF PHYSICAL CHEMISTRY A

Subscriber access provided by Universiteit Utrecht

A: Spectroscopy, Molecular Structure, and Quantum Chemistry

Magnetic Properties of #-Conjugated Hybrid Phenoxyl-Nitroxide Radicals with Extended #-Spin Delocalization

Elena Zaytseva, Daisuke Shiomi, Yury Ten, Yuri V. Gatilov, Alyona Lomanovich, Dmitri V. Stass, Artem S. Bogomyakov, Aixia Yu, Kenji Sugisaki, Kazunobu Sato, Takeji Takui, Elena G. Bagryanskaya, and Dmitrii Mazhukin

J. Phys. Chem. A, **Just Accepted Manuscript** • DOI: 10.1021/acs.jpca.9b11856 • Publication Date (Web): 04 Mar 2020

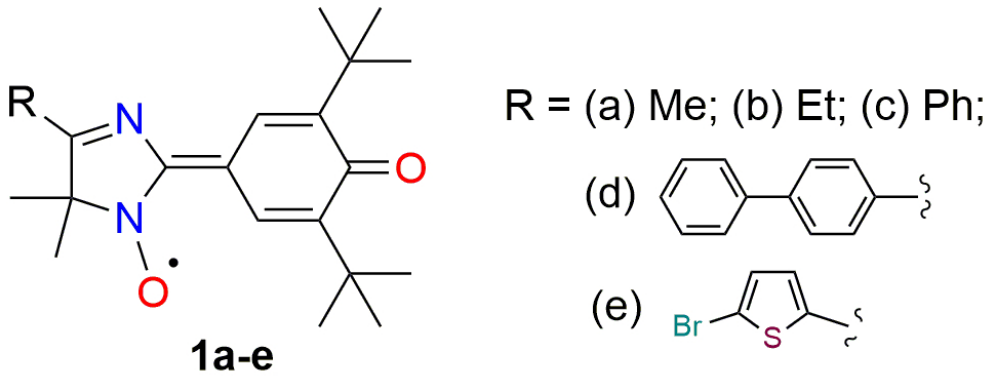

Figure 1. Chemical structure of the conjugated phenoxyl-nitroxides

82x32mm (300 x 300 DPI)

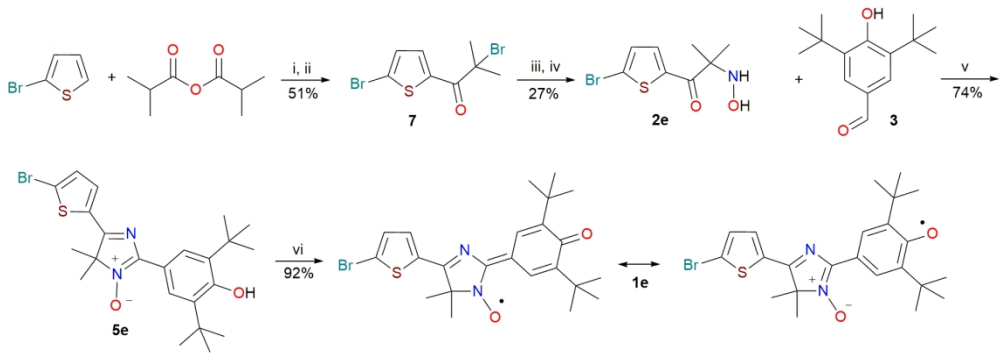

Scheme 1. The synthetic route for hybrid radical 1e with reagents and conditions: (i) BF3×Et2O, 100 °C, 40 min (ii) Br2, Et2O/dioxane, room temperature (rt), 90 min; (iii) NH2OH×HCl, MeONa, MeOH, 65 °C, 8 h; (iv) HClconc., Δ, 15 min; then K2CO3/H2O; (v) NH4OAc, MeOH, Δ, 3 h; then Cu(OAc)2×2H2O, NH3aq, O2, rt, 4h; (vi) PbO2, CHCl3, rt, 30 min.

161x57mm (300 x 300 DPI)

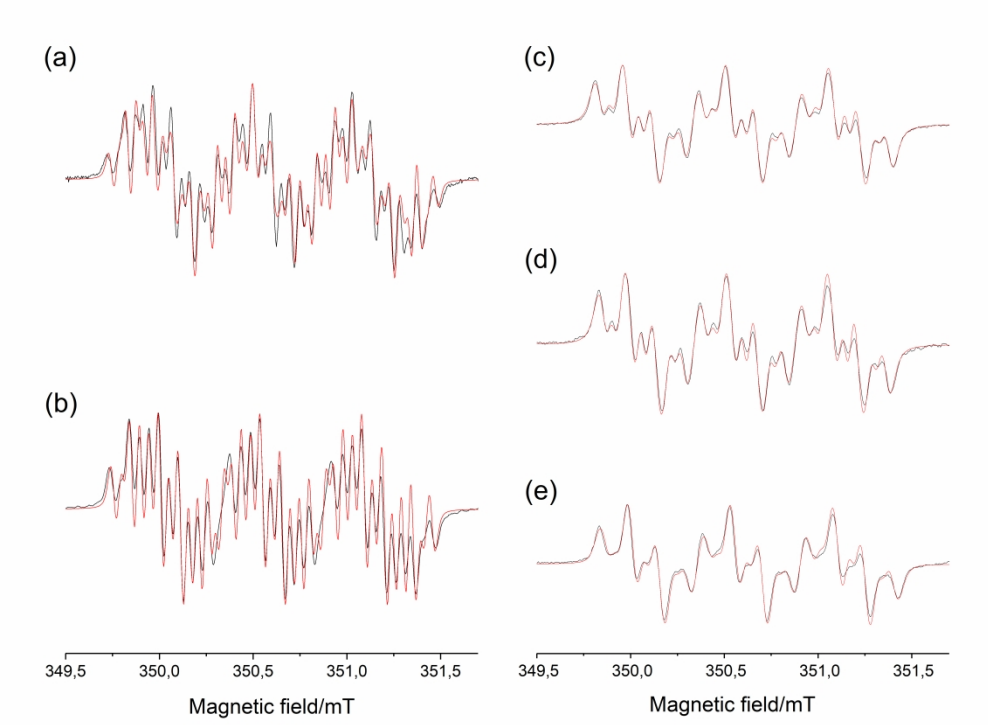

Figure 2. The CW X-band ESR spectra (in black) observed for diluted (10-4 M) and oxygen-free toluene solutions at 295 K of (a) 1a, (b) 1b, (c) 1c, (d) 1d, and (e) 1e. The microwave frequencies used were 9.8748, 9.8749, 9.8748, 9.8750 and 9.8754 GHz for (a), (b), (c), (d) and (e), respectively. The simulated ESR spectra are denoted in red, and the spin Hamiltonian parameters used for the simulation are given in Table 2.

245x181mm (600 x 600 DPI)

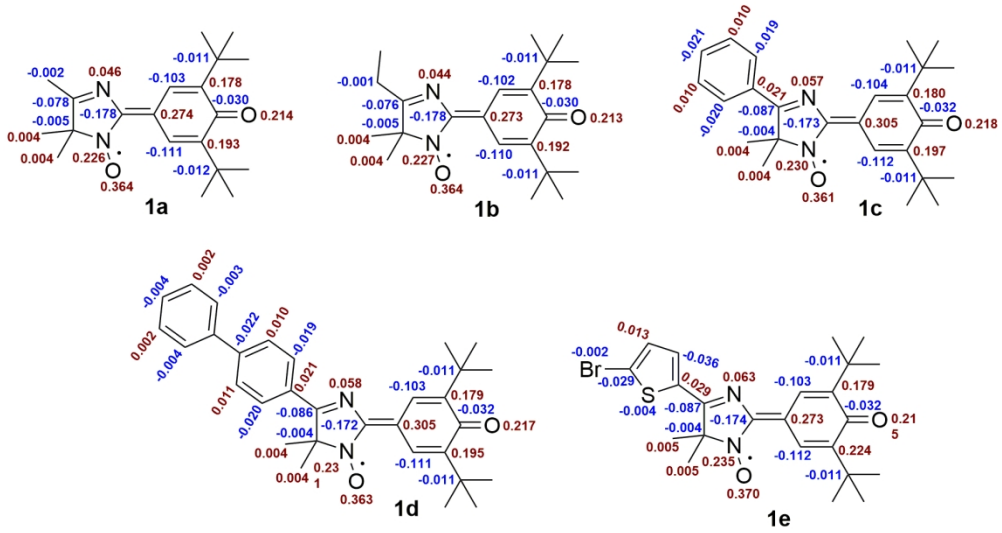

Figure 3. The Mulliken atomic spin populations for 1a-e calculated at the UB3LYP/cc-PVDZ level of theory.

160x86mm (300 x 300 DPI)

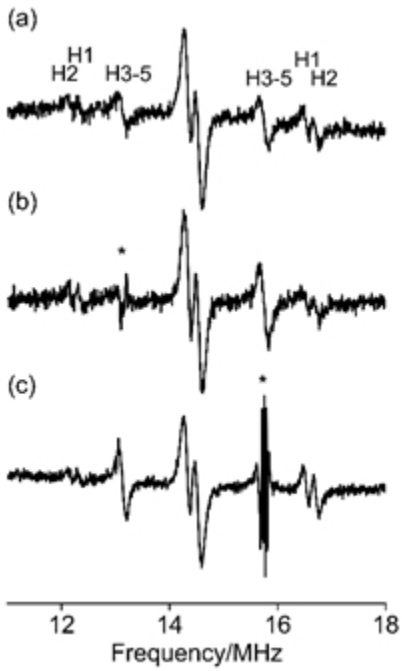

Figure 4. 1H-ENDOR and TRIPLE spectra of 1a in toluene observed at 298 K. (a) A 1H ENDOR spectrum observed with the static magnetic field at 338.6275 mT; (b) and (c) TRIPLE spectra obtained by pumping the ENDOR transitions by the second radio frequency (RF) irradiation. An asterisk indicates the second RF irradiation for the pumping. The pumping frequencies in (b) and (c) are 13.124 and 15.734 MHz, respectively. In (b), when the second RF pumps (*) at the ENDOR line of 13.124 MHz, the intensity of the corresponding H3-5 ENDOR line appearing at 15.7734 MHz increases in comparison with the intensity without the irradiation (see Fig. 4(a)). On the other hand, the intensities of the ENDOR lines denoted by H1 and H2 decrease in comparison with those without the irradiation. In (c), the situations are inverse when the line at 15.774 MHz is pumped. Thus, the relative sign of the hfcc's for H1 (and H2) is opposite to that of H3-5.

57x93mm (96 x 96 DPI)

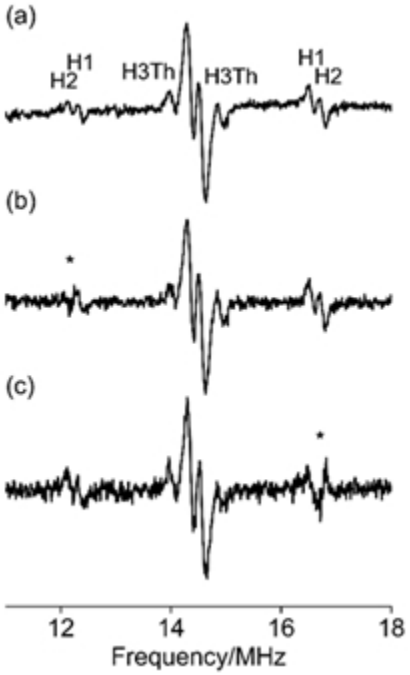

Figure 5. 1H-ENDOR and TRIPLE spectra of 1e in toluene observed at 298 K. (a) A 1H ENDOR spectrum observed with the static magnetic field at 338.6212 mT; (b) and (c) TRIPLE spectra obtained by pumping the ENDOR transitions by the second radio frequency (RF) irradiation. An asterisk indicates the second RF irradiation for the pumping. The pumping frequencies in (b) and (c) are 12.176 and 16.719 MHz, respectively. In (b), when the second RF pumps (*) at the ENDOR line of 12.176 MHz, the intensity of the corresponding H3Th ENDOR line appearing at 14.86 MHz increases in comparison with the intensity without the irradiation (see Fig. 5 (a)) . The intensities of the ENDOR lines denoted by H1 and H2 around 16.7 MHz also increase in the same way. In (c), the situations are inverse when the line at 16.719 MHz is pumped. Thus, the relative sign of the hfcc for H3Th is the same as those of H1 and H2.

57x93mm (96 x 96 DPI)

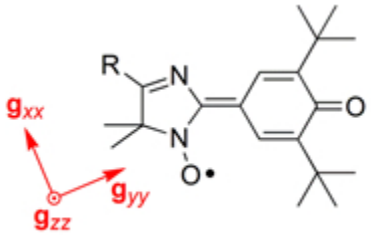

Figure 6. Relationship between the theoretical g tensors and molecular structures in the hybrid radicals, 1a-e.

57x37mm (96 x 96 DPI)

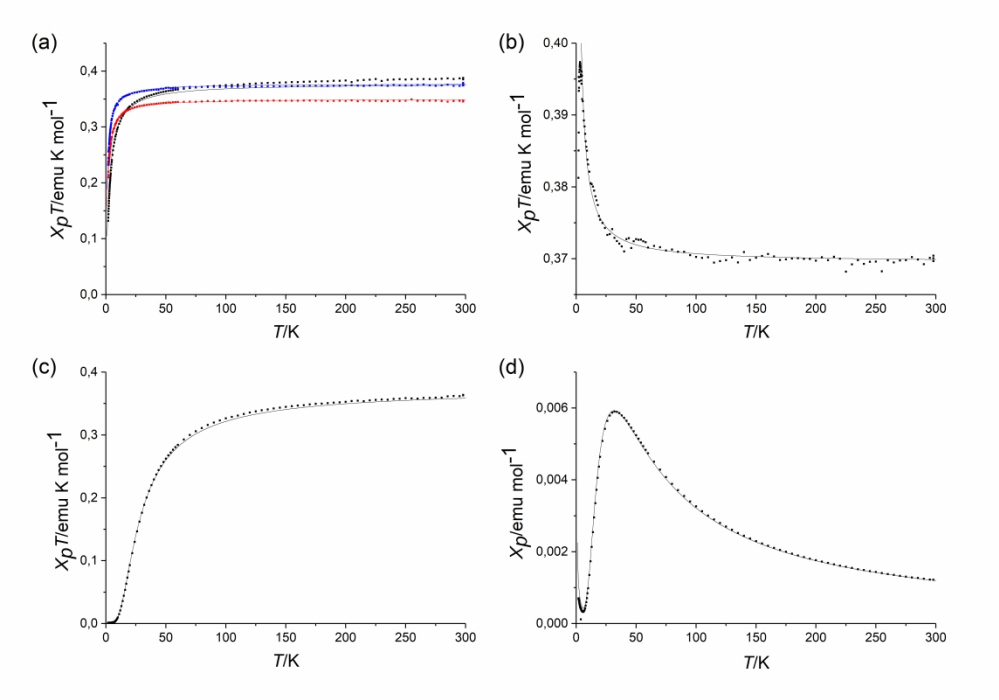

Figure 7. The SQUID magnetometry of the polycrystalline (solid) radicals 1a-e: (a), (b) and (c) χparaT vs. T χpara vs. T plots for (a) 1a (black);, 1b (red); 1d (blue); (b) 1c; (c) and (d) 1e. The dotted curves denote the experimental values and the solid curves the calculated Curie-Weiss curves in (a),(b) or Bleany-Bowers curve (J/kB = -25.6 K + Curie curve in (c) and (d).

261x184mm (600 x 600 DPI)

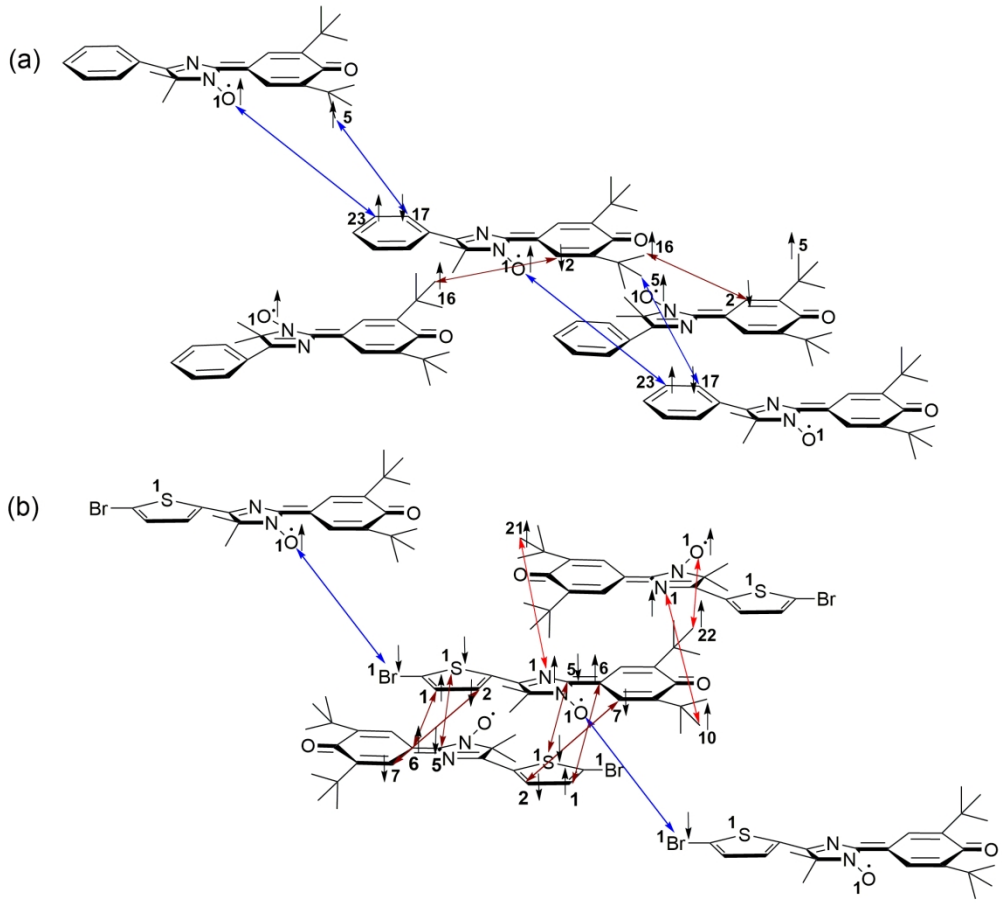

Figure 8. The short contacts in the single crystals of (a) 1c and (b) 1e. The blue arrows represent contacts in the ferromagnetic head-over-tail chains and the red ones - contacts in the antiferromagnetic head-to-tail dimers.

185x168mm (300 x 300 DPI)

Magnetic Properties of π-Conjugated Hybrid Phenoxyl-Nitroxide Radicals with Extended π-Spin Delocalization

Elena Zaytseva,[a,b] *Daisuke Shiomi,*[c] *Yury Ten,* [a]*Yuri V. Gatilov,*[a,b] *Alyona Lomanovich,*[a] *Dmitri Stass,*[b, d] *Artem Bogomyakov,*[b,e] *Aixia Yu,*[b] *Kenji Sugisaki,*[c] *Kazunobu Sato,*[*c] *Takeji Takui,*[*c, f] *Elena Bagryanskaya*[a,b] *and Dmitrii Mazhukin*[*a,b]

a. N.N. Vorozhtsov Novosibirsk Institute of Organic Chemistry SB RAS, 9 Acad. Lavrentyeva Ave., Novosibirsk, 630090, Russia.

b. Novosibirsk State University, 2 Pirogova Str., Novosibirsk, 630090, Russia

c. Department of Chemistry and Molecular Materials Science, Graduate School of Science, Osaka City University, 3-3-138 Sugimoto, Sumiyoshi-ku, Osaka 558-8585, Japan.

d. Voevodsky Institute of Chemical Kinetics and Combustion SB RAS, 3 Institutskaya Str., Novosibirsk, 630090, Russia

e. International Tomography Center SB RAS, 3 Institutskaya Str., Novosibirsk, 630090, Russia

f. Research Support Department/University Research Administrator Center, University Administration Division, Osaka City University, 3-3-138 Sugimoto, Sumiyoshi-ku, Osaka 558-8585, Japan

ABSTRACT A series of stable and genuinely organic open-shell systems, π-conjugated phenoxyl-nitroxide free radicals (hybrid phenoxyl-nitroxide radicals) have been synthesized and their magnetic properties in the crystalline state investigated, revealing their usefulness of new building blocks for molecular magnetic materials. The salient electronic structure of the hybrid phenoxyl-nitroxide radicals is extended π-spin delocalization from the nitroxide moiety, mediating the localization effect intrinsic to nitroxide radicals. Five representative hybrid radicals containing an aliphatic, aromatic and heteroaromatic substituent in the side part of the compact hybrid radical centers were synthesized, and their molecular/crystal structures in the crystalline state were determined by X-Ray diffraction analyses. CW X-band ESR, ^{1}H-ENDOR spectroscopy and DFT calculations for the hybrid radicals confirmed that an unpaired spin delocalizes over the whole molecular frame including the non-conjugated fragments, suggesting the possibility of tuning their electronic properties through substituent effects in the crystalline state. Significant influence of the phenoxyl moiety on the electronic structure was analyzed in terms of the g-tensor calculations. The SQUID magnetization measurements revealed that the nitroxides bearing alkyl or aromatic substituents behave as 3D Curie-Weiss paramagnets with weak antiferromagnetic (AFM) (Θ = -1÷-2.6 K) or ferromagnetic (FM) (Θ = +0.33 K) spin-spin exchange interactions. On the other hand, heteroaromatically substituted hybrid phenoxyl-nitroxide showed significant AFM interactions with J/k_B = -25.6 K. The analysis of the bulk magnetic properties based on the crystallographic data and DFT calculations revealed competition between the intermolecular AFM and FM interactions which originate from the C-

O(phenoxyl)...Me(nitroxide) or (N)O-C(arom) infinite 1D head-to-tail chains and the C(arom)-C(arom) head-over-tail dimers forming 3D networks in their crystal lattices.

1. INTRODUCTION

Resonance stabilized hybrid organic free radicals, in which π-conjugation extending to nitroxide is topologically controlled, seem to be good candidates as building blocks for designing advanced organic magnetic materials due to their highly delocalized unpaired spin and, as a result, increasing the possibilities of magnetic coupling through numerous pathways, consequently leading to a chance for bulk magnetic ordering in the crystalline state.[1-3] A variety of crystalline organic molecule-based ferro- or ferri-magnets[4-15] have been documented since the first organic ferromagnet appeared in 1991.[4]

Among efforts to acquire advanced molecule–based magnetic materials, rational molecular designs of component organic open shell entities have been crucial, and important attempts have been made[16-25]. Moreover, the more extensive the unpaired spin delocalization is, the larger will be the impact of substituent effects on the tuning of molecular electronic properties, underlain by exchange interactions in the crystalline state.[26, 27] Recently, conjugated heavy atom heterocyclic radicals have been shown to be applicable as advanced conductive and magnetic materials as a consequence of easily tunable spin distributions and the ability to modify their crystal packing.[26, 28, 29] We note, however, that due to the persistence of such radicals and complicated synthetic procedures to obtain them, to date the diversity of the hybrid organic radicals is rather poor. In this work, we have synthesized a series of stable all-organic hybrid nitroxides **1** (Fig. 1), in which phenoxyl is compactly π-conjugated, as new potential building blocks of advanced

organic magnetic materials. Built as a hybrid of two well-known classes of organic free radicals: nitroxides and phenoxyls, these molecules represent a family of paramagnetic compounds where the unpaired electron delocalizes over both the NO site and the phenoxyl ring due to the connectivity (topological symmetry) of the π-electron network.

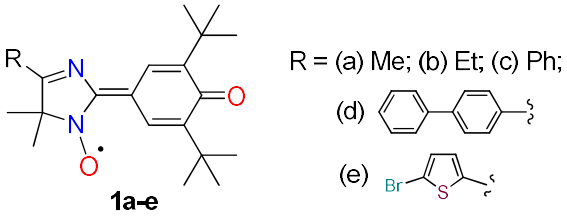

Figure 1. Chemical structure of the conjugated phenoxyl-nitroxides

Importantly, the stability of phenoxyl-nitroxides arises from both the steric hindrance induced by bulky *tert*-butyl groups near the phenoxyl site and the efficient delocalization of the unpaired electron over the molecular frame.[30] It should be noted that the union of a sterically hindered phenol with the strong acceptor 4*H*-imidazole 3-oxide moiety gives sufficient stabilization for the hybrid paramagnetic molecule, while the presence of other heterocyclic substituents at the C-4 of the phenol ring does not lead to significant radical stabilization.[31] It is essential that the presence of the *tert*-butyl groups changes the geometry of the hybrid radicals making them non-planar which influences their crystal packing mode and destroys the symmetry of the head-over-tail π-π-dimers typically formed by flat conjugated compounds in the crystalline state.[32] The subtle geometrical changes significantly influence the macroscopic magnetic properties, controlled not only by the absolute values of spin density on contacted atoms but also by the distances between them and the numbers of such contacts in the pair of radicals.

Despite the fact that the first representatives of hybrid phenoxyl nitroxides were recently announced by us,[33] there has been no attempt to study their magnetic properties thoroughly. Thus, the purpose of this work is to identify the salient electronic features of compactly π-

conjugated hybrid radicals and to understand how the spin distribution and crystal packing mode occurring in the crystals of hybrid phenoxyl-nitroxides influence their bulk magnetic properties in order to guide the use of this class of paramagnetic compounds as building blocks for genuinely organic magnetic materials.

2. EXPERIMENTAL

General. Analytical and spectroscopic studies were performed in the Multi-Access Chemical Research Center SB RAS for spectral and analytical measurements. Analytical-grade reagents and solvents were purchased from Acros Organics or Alfa-Aesar. Column chromatography and TLC were performed using Acros silica gel 60A (0.035–0.070 mm) and Sorbfil PTLC-AF-UV 254 (Russia), respectively. ^{1}H NMR and ^{13}C NMR spectra were recorded on Bruker AV-400 and DRX-500 spectrometers at 400/500 and 100/125 MHz, respectively, for 1–5% solutions of compounds in $CDCl_3$. Fourier transform infrared (FT-IR) spectra were acquired in KBr pellets on a Bruker Vector-22. The UV-Vis spectra were obtained for EtOH solutions using a Hewlett-Packard HP 8453 spectrophotometer. Elemental analyses were performed on an automatic CNS analyzer Euro EA 3000. The melting points were determined on a Mettler Toledo FP 81 HT instrument.

Synthesis. As an example, we present here a complete synthesis of hybrid radical **1e**, which was obtained in seven stages, based on commercially available 2-bromothiophene (Scheme 1). Acylation of the latter with *iso*-butyric acid anhydride in the presence of boron trifluoride etherate afforded corresponding ketone, 1-(5-bromothiophen-2-yl)-2-methylpropan-1-one **6**. Subsequent halogenation of this compound followed by interaction of bromoketone **7** with a fivefold excess of hydroxylamine, and hydrolysis of the intermediate 2-hydroxylamine oxime **8** by boiling with concentrated hydrochloric acid lead to 2-(hydroxylamino)ketone hydrochloride.

We have found that the condensation of its free base ketone **2e** with aldehyde **3** in the presence of ammonium acetate leads to an inseparable mixture of 2,5-dihydroimidazole **4e** and acyclic ketonitrone, which was converted with a high yield into the target 4*H*-imidazole 3-oxide **5e** by one-pot oxidation of the resulting mixture with oxygen in the presence of copper acetate. Hybrid phenoxyl nitroxyl radical **1e** was formed with a yield of more than 90% when imidazole **5e** was treated with a six fold excess of PbO_2. Synthetic procedures for hybrid radicals **1a-c** and intermediates **2e, 4a-c, 5c, 5e, 6, 7** are presented in Supplementary Information. Compound **1d** was prepared and characterized previously.[33]

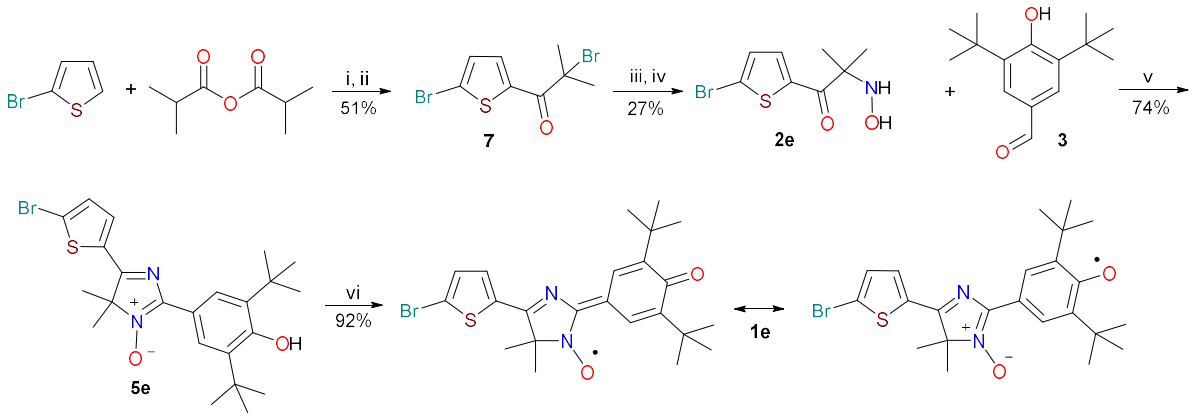

Scheme 1. The synthetic route for hybrid radical **1e** with reagents and conditions: (i) $BF_3 \times Et_2O$, 100 °C, 40 min (ii) Br_2, Et_2O/dioxane, room temperature (rt), 90 min; (iii) $NH_2OH \times HCl$, MeONa, MeOH, 65 °C, 8 h; (iv) $HCl_{conc.}$, Δ, 15 min; then K_2CO_3/H_2O; (v) NH_4OAc, MeOH, Δ, 3 h; then $Cu(OAc)_2 \times 2H_2O$, NH_3aq, O_2, rt, 4h; (vi) PbO_2, $CHCl_3$, rt, 30 min.

Crystallographic study. Single crystals of **1a-c**, **e** were obtained by slow cooling of their diluted solutions in acetonitrile. The X-ray diffraction study revealed that **1a-e** have almost flat molecular structures and the dihedral angles between the nitroxide and phenoxide planes are within the interval of 2.3° (**1e**) – 7.7° (**1c**). In crystals of **1a** and **1b** the molecules are located on a C2 axis passing through C=O bonds and, as a result, disordered. The bond lengths in **1a-c**, **e** are

close to the corresponding bond lengths in **1d**,[33] except those in the disordered fragments. The crystallographic data on **1a-c**, **e** are given in Table 1.

Table 1. The crystallographic data for **1a-c**, **e**

Parameters	**1a**	**1b**	**1c**	**1e**
Formula	$C_{20}H_{29}N_2O_2$	$C_{21}H_{31}N_2O_2$	$C_{25}H_{31}N_2O_2$	$C_{23}H_{28}BrN_2O_2S$
Formula Weight, F(000)	329.45, 1432	343.48, 1496	391.52, 844	476.44, 1976
Crystal System	Orthorhombic	Orthorhombic	Orthorhombic	Monoclinic
Space group	Fdd2	Fdd2	$Pna2_1$	C2/c
Temperature/K	296(2)	296(2)	200(2)	296(2)
a/ Å, *b*/Å *c*/Å	16.3593(17), 21.004(3), 11.7496(17)	21.6081(16), 16.5776(9), 11.8413(7)	11.292(2), 10.4647(14), 18.345(3)	20.2830(16), 11.8216(7), 20.3949(16)
β/deg, volume/Å^3	90, 4037.2(10)	90, 4241.7(5)	90, 2167.8(6)	101.691(3), 4788.8(6)
Z, density/g/cm^3	8, 1.084	8, 1.076	4, 1.200	8, 1.322
μ/mm^{-1}, θ_{max}/deg	0.070, 25.2	0.069, 25.1	0.076, 26.0	1.824, 27.2
h,*k*,*l* max	19, 24, 14	24, 19,14	13, 11, 22	26, 15, 26
Reflections all, unique	15849, 1798	16790, 1896	6501, 3881	25891, 5306
R_{int}, observed $I>2\sigma$	0.0222, 1220	0.0427, 1316	0.0397, 3100	0.0613, 3829
*N*par, wR_2 (all)	147, 0.1582	138, 0.3046	271, 0.0777	270, 0.1057
R ($I>2\sigma$), *S*	0.0510, 1.130	0.0767, 1.188	0.0345, 0.941	0.0437, 0.961
CCDC	1953101	1953102	1953103	1953104

X-ray diffraction measurements. The diffraction data were collected on a Bruker KAPPA APEX II CCD area-detector diffractometer equipped with a graphite monochromated Mo-Kα

radiation (λ = 0.71073 Å). The unit cell parameters were determined from a least-squares refinement of the setting angles. The structure was solved by direct methods and refined on F^2 by the full-matrix least-squares methods with SHELXS-97. The refinement was carried out by full-matrix least squares method on the positional and anisotropic temperature parameters of the non-hydrogen atoms using SHELXL-97. All H atoms were placed in the idealized positions and constrained to ride on their parent atoms. Geometrical restrictions were applied for disordered part of **1a**, **b** molecules. Crystallographic data for compounds **1a-c**, **e** were deposited at CCDC center and can be obtained free of charge from The Cambridge Crystallographic Data Centre via www.ccdc.cam.ac.uk/ data_request/ cif.

ESR and ^{1}H-ENDOR/TRIPLE measurements. CW X-band ESR spectra were obtained in diluted and oxygen free toluene solutions at 295 K at the concentrations of ~10^{-4} M on a Bruker X Band (9 GHz) spectrometer Elexys E 540. Experimental CW ESR settings were as follows: microwave power, 2.0 mW; modulation frequency, 100 kHz; modulation amplitude, 0.02-0.03 mT; time constant, 300 ms; sweep time, 300 s; number of points, 1024; number of scans, 1. For determining the isotropic *g*-values (g_{iso}), we recorded X-band CW ESR spectra of mixtures of the investigated radical with Finland trityl. Then the known g_{iso} of Finland trityl was used for the spectrum simulation, and the target g_{iso} value was determined. The simulations of the solution ESR lines were carried out in the software package EasySpin which is available at www.easypin.org ^{1}H-ENDOR/TRIPLE (Electron-Nuclear-DOuble-Resonance/ electron-nuclear-nuclear TRIPLE resonance) spectra of **1a** and **1e**, as representative hybrid radicals, in toluene were observed at 298 K on a Bruker ESP300/350 spectrometer.

SQUID measurements. The magnetic susceptibility was measured for randomly oriented polycrystalline samples on a Quantum Design SQUID magnetometer MPMS-XL at magnetic

field of 0.1 T up to 1.5 T, depending on the compounds. The linearity of magnetization *M* vs. magnetic field *B* at the specific field has been checked prior to temperature variation measurements.

DFT calculations. The geometries of **1a-e** were optimized at the UB3LYP/cc-pVDZ level of theory. Starting geometries for **1a-e** were their solid state structures. The solvent effect was modeled by the CPCM method (solvent – toluene). The calculations were executed with the Gaussian 09 program package.[34] Spin density distribution maps and orbital's visualizations were acquired by means of Chemcraft program.

Broken-symmetry DFT calculations were performed to compute parameters *J* of the exchange interactions ($\widehat{\boldsymbol{H}} = -\mathbf{2}\boldsymbol{J}\widehat{\boldsymbol{S_1}}\widehat{\boldsymbol{S_2}}$) between the radicals with close contacts in the crystals lattices of **1a-e**. The calculations were performed using Orca software package[35] with the unrestricted B3LYP functional and the def2-TZVP basis sets. The mutual orientations of the radicals and their geometries were extracted from their single crystal X-ray diffraction data and used without any further optimizations.

3. RESULTS AND DISCUSSION

3.1. Spin density distribution in 1a-e by CW ESR, ^{1}H-ENDOR spectroscopy and DFT calculations

CW X-band ESR spectra measured for diluted and oxygen-free toluene solutions of **1a-e** at room temperature are shown in Fig. 2; the observed and simulated spectra given in black and red, respectively. The observed signals consist of complex multiplets with g_{iso} = 2.0056, which can be well reproduced using a model based on hyperfine structures due to two distinct ^{14}N and many ^{1}H nuclei. In the case of **1a**, **b** the ^{1}H nuclei of the side methyl and ethyl group also should be taken into account for the spectral simulations. The experimental hyperfine coupling constants

(hfcc's) for the ^{14}N (a_N) and ^{1}H nuclei (a_H) derived on the basis of the ESR hyperfine spectral simulations are listed in Table 2.

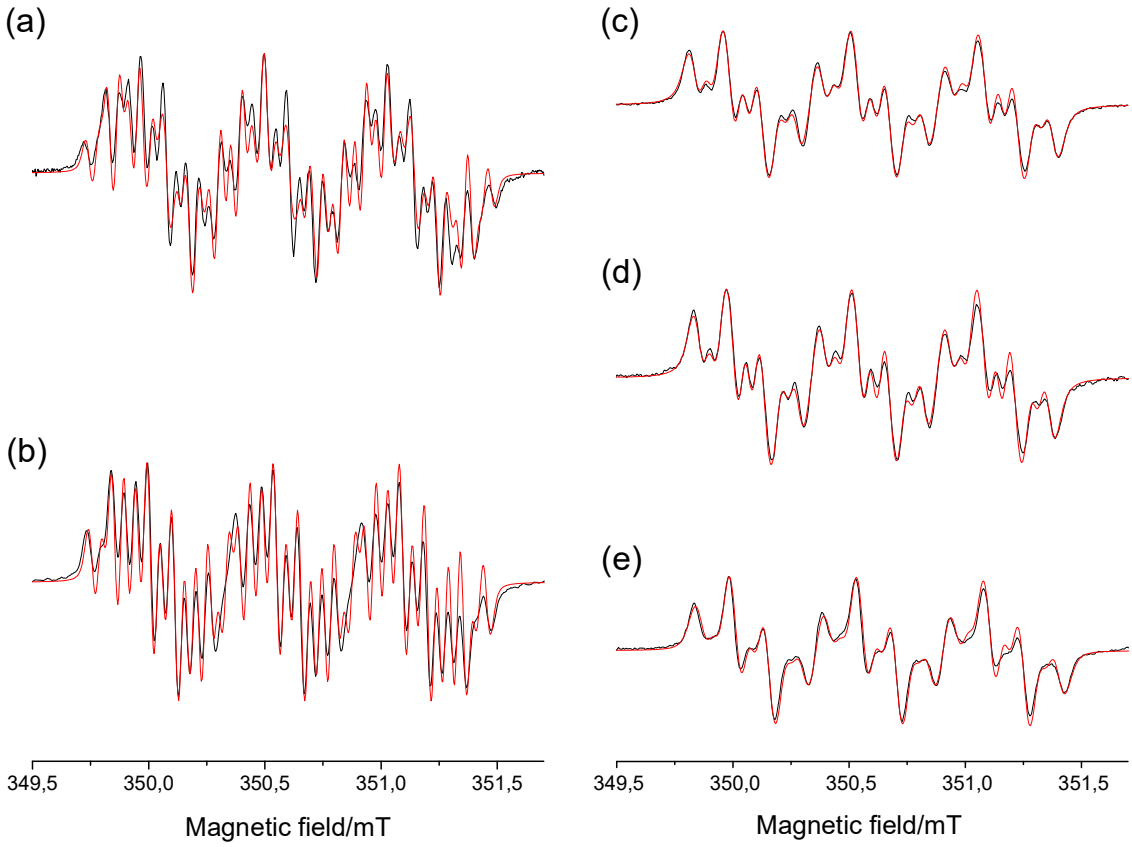

Figure 2. The CW X-band ESR spectra (in black) observed for diluted (10^{-4}M) and oxygen-free toluene solutions at 295K of (a) **1a**, (b) **1b**, (c) **1c**, (d) **1d**, and (e) **1e**. The microwave frequencies used were 9.8748, 9.8749, 9.8748, 9.8750 and 9.8754 GHz for (a), (b), (c), (d) and (e), respectively. The simulated ESR spectra are denoted in red, and the spin Hamiltonian parameters used for the simulation are given in Table 2.

Table 2. The experimentally determined spin Hamiltonian parameters for **1a-e** from their ESR spectra simulations and the calculated ones (UB3LYP/cc-PVDZ). Note that we determined the

isotropic ^{1}H-hyperfine coupling parameters of **1a** from its ^{1}H-ENDOR/TRIPLE spectra; a_{H1} = 4.178 MHz (a' = $a/g\beta$ = 0.149 mT), a_{H2} = 4.531 MHz (0.161 mT), $a_{H3,4,5}$ = -2.621 MHz (0.093 mT), and $|a(\text{others})| \leq 0.3$ MHz (0.010 mT). The relative signs of the experimental hyperfine coupling constants were determined by the TRIPLE spectroscopy.

Compound	g_{iso}	a_{N1}/mT	a_{N2}/mT	a_{H1}/mT	a_{H2}/mT	$a_{H3,4,(5)}$/mT	Linewidth (peak-to-peak)/mT
1a Exp.	2.0056	0.560	0.053	0.151	0.167	0.090	0.042
Calcd.	2.0062	0.598	0.109	0.188	0.204	-0.181	
1b Exp.	2.0056	0.558	0.054	0.152	0.171	0.097	0.047
Calcd.	2.0062	0.598	0.106	0.187	0.203	-0.247	
1c Exp.	2.0056	0.551	0.062	0.156	0.160	-	0.075
Calcd.	2.0063	0.607	0.137	090	0.206		
1d Exp.	2.0056	0.553	0.062	0.156	0.157	-	0.072
Calcd.	2.0064	0.611	0.170	0.188	0.204		
1e Exp.	2.0056	0.548	0.065	0.152	0.154	-	0.076
Calcd.	2.0060	0.623	0.105	0.189	0.205		

For the better understanding of the spin density distributions in the hybrid radicals **1a-e**, DFT calculations of the magnetic properties at the UB3LYP/cc-pVDZ level of theory were performed using the single crystal geometries of **1a-e** as starting points for molecular structural optimizations. The calculated values of the hfcc's are listed also in Table 2. Note that H1 and H2 are assigned to the two phenoxyl ring protons and three protons denoted by H3,4,5 assigned to the methyl protons of the imidazole moiety, and the numbering for the protons is for convenience. We have attempted to experimentally determine the relative signs of the hfcc's of the protons by using CW X-band ^{1}H ENDOR/TRIPLE (Electron-Nuclear-DOuble

Resonance)/Electron-Nuclear-Nuclear TRIPLE resonance) spectroscopy, as discussed below. Although the absolute values of the calculated hfcc's are slightly overestimated in comparison with the corresponding experimental ones, the main feature of the spin density distribution is reproduced well. Note that the overestimation is related to the functional (see SI for the details). The calculated SOMO orbitals and spin density distribution maps for **1a-e** are depicted on Fig. 3, and Figs. S14 and S15 (See SI part), correspondingly. It is clear from Figs. S14 and S15 that the spin density is distributed over the whole molecular frame. The main part of an unpaired electron population is distributed toward the conjugated nitroxide-phenoxyl fragment so as the spin densities on the heteroatoms have positive signs, leading to the comparable hfcc's in the absolute values for the ^{14}N nuclei (See Fig. 3). The electronic structure of the hybrid radicals, in which the heteroatoms also are included in the π-conjugation, is mainly governed by the topological symmetry of the π-electron network.[1, 36] The minor part of the unpaired electron population also extends over the non-conjugated fragment of **1a-e**. Here, depending on the substituent, aliphatic or aromatic, the spin density is localized on the CH_2 group or delocalized over the aromatic ring (the spin network is π-topologically controlled). More specifically, in **1d** the electron spin is delocalized on the biphenyl ring bonded to the imidazole moiety, and in **1e** the spin density on the sulphur atom is negative in sign and negligible.

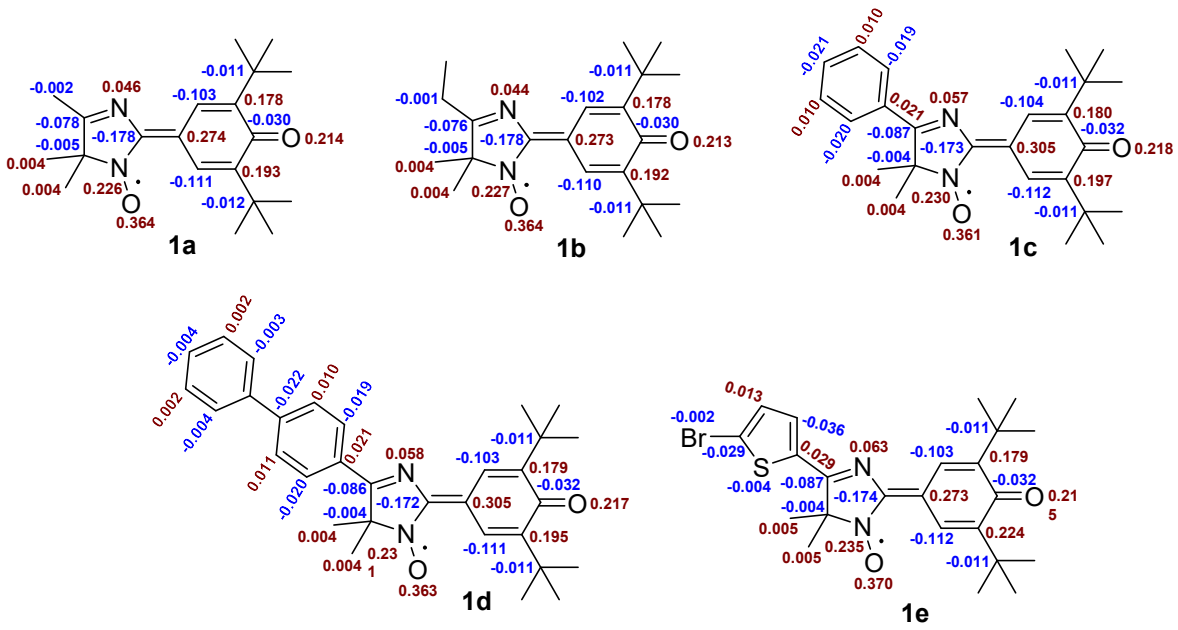

Figure 3. The Mulliken atomic spin populations for **1a-e** calculated at the UB3LYP/cc-PVDZ level of theory.

The observed ^{1}H-ENDOR and TRIPLE spectra of the representative hybrid radical **1a** in toluene at room temperature are shown in Fig. 4. The ^{1}H-hyperfine splitting due to H1, H2 (phenoxyl ring), and H3-5 (methyl) protons were distinctly observed. The strong ^{1}H-ENDOR signals observed near the free-proton NMR frequency ν_n (= 14.442 MHz) are attributed to the other weakly coupled protons. The TRIPLE spectra in Figs. 4(b) and (c) clearly show that the sign of the hfcc's of H3-5 is opposite to those of H1 and H2. The isotropic hfcc's for the protons of **1a** determined from the ENDOR/TRIPLE spectra are as follows; a_{H1} = +4.178 MHz (a' = $a/g\beta$= +0.149 mT), a_{H2} = +4.531 MHz (+0.161 mT), $a_{H3\text{-}5}$ = -2.621 MHz (-0.093 mT), and $|a(\text{others})| \leq 0.3$ MHz (0.01 mT).

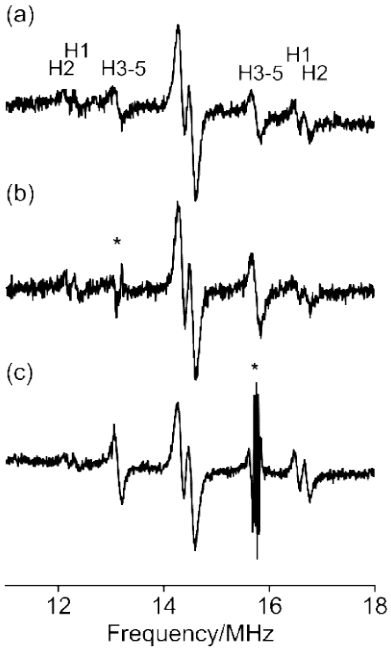

Figure 4.[1]H-ENDOR and TRIPLE spectra of **1a** in toluene observed at 298 K. (a) A [1]H ENDOR spectrum observed with the static magnetic field at 338.6275 mT; (b) and (c) TRIPLE spectra obtained by pumping the ENDOR transitions by the second radio frequency (RF) irradiation. An asterisk indicates the second RF irradiation for the pumping. The pumping frequencies in (b) and (c) are 13.124 and 15.734 MHz, respectively. In (b), when the second RF pumps (*) at the ENDOR line of 13.124 MHz, the intensity of the corresponding H3-5 ENDOR line appearing at 15.7734 MHz increases in comparison with the intensity without the irradiation (see Fig. 4(a)).On the other hand, the intensities of the ENDOR lines denoted by H1 and H2 decrease in comparison with those without the irradiation. In (c), the situations are inverse when the line at 15.774 MHz is pumped. Thus, the relative sign of the hfcc's for H1 (and H2) is opposite to that of H3-5.

The observed [1]H-ENDOR and TRIPLE spectra of the hybrid radical **1e** were given in Fig. 5. In addition to the [1]H-hyperfine splittings due to H1, H2 (phenoxyl ring protons), the splitting due to

the proton (H3Th, 3-H Th) in the thiophene ring was observed, which was not resolved in the CWESR spectrum. The hfcc's for the protons of **1e** were determined as follows: a_{H1} = +4.199 MHz (+0.150 mT), a_{H2} = +4.548 MHz (+0.162 mT), a_{H3Th} = +0.817 MHz (+0.029 mT), and $|a(\text{others})| \leq 0.3$ MHz (0.01 mT). As shown in Figs. 5(b) and (c), the TRIPLE spectra show that

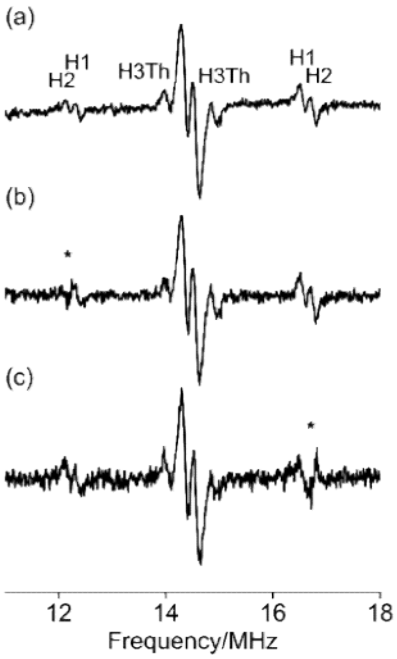

all the protons (H1, H2, and H3Th) have the same sign of the hfcc's.

Figure 5. ^{1}H-ENDOR and TRIPLE spectra of **1e** in toluene observed at 298 K. (a) A ^{1}H ENDOR spectrum observed with the static magnetic field at 338.6212 mT; (b) and (c) TRIPLE spectra obtained by pumping the ENDOR transitions by the second radio frequency (RF) irradiation. An asterisk indicates the second RF irradiation for the pumping. The pumping frequencies in (b) and (c) are 12.176 and 16.719 MHz, respectively. In (b), when the second RF pumps (*) at the ENDOR line of 12.176 MHz, the intensity of the corresponding H3Th ENDOR line appearing at 14.86 MHz increases in comparison with the intensity without the irradiation (see Fig. 5 (a)) . The intensities of the ENDOR lines denoted by H1 and H2 around 16.7 MHz also increase in the

same way. In (c), the situations are inverse when the line at 16.719 MHz is pumped. Thus, the relative sign of the hfcc for H3Th is the same as those of H1 and H2.

We emphasize that the ^{1}H ENDOR/TRIPLE spectroscopy is capable of giving unambiguous identification of key hfcc's for protons, enabling us to discuss the electronic structures of complex radicals in a straightforward manner with the aid of theoretical considerations.

3.2. Salient features of hybrid radicals, phenoxyl-nitroxides 1a-e as derived from the observed isotropic *g*-values and their theoretical analysis

To reveal the salient features of the electronic structures of **1a-e** in more detail, the g tensor calculations were performed at the UB3LYP/cc-pVDZ level using ORCA (Version 4.0.1.2) software.[35] The theoretical g tensors of **1a-e** are summarized in Table 3, and relationship between the principal axes of the theoretical g tensors and molecular structures are illustrated in Fig. 6. The isotropic g values are also listed in Table 2 for comparison with the experimental values. The optimization for the molecular structures was carried out, where the initial structures were taken from those given in Fig. S14 (See SI part).

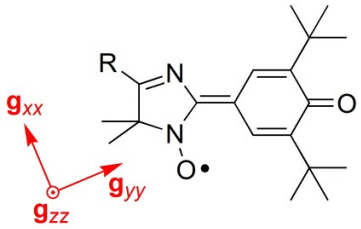

Figure 6. Relationship between the theoretical g tensors and molecular structures in the hybrid radicals, **1a-e**.

Table 3. The theoretical g tensors of **1a-e** calculated at the UB3LYP/cc-pVDZ level.

Molecule	g_{xx}	g_{yy}	g_{zz}	g(iso)
1a	2.0086	2.0077	2.0023	2.0062
1b	2.0086	2.0077	2.0023	2.0062
1c	2.0085	2.0079	2.0023	2.0063
1d	2.0086	2.0082	2.0024	2.0064
1e	2.0079	2.0076	2.0026	2.0060

The theoretical isotropic *g*-values of **1a-e** range from 2.0060 to 2.0064, are overestimated compared with the experimental ones. As pointed out above, the overestimation of the isotropic *g*-values similarly is functional-dependent. B3LYP tends to overestimate the isotropic *g*-values, while B97-D reproduces the experimental ones (see SI for the details). There is no significant solvent (toluene) effect on the **g**-tensors. The direction of the largest principal *g*-value denoted by g_{XX} in Fig. 6 and Table 3 for each phenoxyl-nitroxide is nearly parallel to that of the N-O bond, indicating that the spin-orbit interaction due to the NO site is predominant and the electronic excitation to SOMO from the in-plane 2p lone pair located at the oxygen atom of the NO site significantly contributes to the deviation from the free electron *g*-value of 2.0023 (g shift).

The direction of the principal value g_{yy} lies in the molecular plane and perpendicular to the N-O bond, indicating that the excitation to SOMO from the in-plane 2p lone pair orbital at the oxygen atom of the phenoxyl moiety contributes to the *g* shift. The direction of the principal g_{zz} value is perpendicular to the molecular plane. Indeed, the directions of the principal g_{xx} or g_{yy} values depend on the substituent R (in Figs. 1 and 6), but only change 10 – 20 degrees in the molecular plane for the hybrid radicals under study. This is consistent with the fact that the structures of SOMOs of the phenoxyl-nitroxides are very similar each other (Fig.S14).

Particularly, we refer to the theoretical g_{yy} values and the overestimation of the isotropic *g*-values. The calculated g_{yy} values for the hybrid radicals under study are about 2.0078 and they are considerably larger than those of typical nitroxide radicals (g_{yy} ~ 2.006).[37] Importantly, the larger g_{yy} shift can be explained in terms of the existence of sizable spin–orbit coupling on the oxygen atom of the phenoxyl moiety. The theoretical isotropic *g*-values are slightly overestimated from the experimentally determined ones.

It is known that the B3LYP functional has a tendency to overestimate the spin delocalization effects[38] and the theoretical hyperfine coupling constant a_H for the protons of the phenyl group are larger than the corresponding experimental values. Thus, we note that the current calculations overestimate the spin delocalization onto the phenoxyl moiety.

Macroscopic magnetic properties of 1a-e in the crystalline state

The temperature dependence of paramagnetic susceptibility $\chi_{para}$is represented on Fig. 7a-d. Theχ_{para} values were determined as a difference between the corresponding χ_M and temperature-independent diamagnetic susceptibilities, χ_{dia}. Theχ_{dia} values were calculated using Pascal`s scheme and listed in Table 4. The$\chi_{para}T$ vs. *T* plots for **1a, b, d** can be well fitted using Curie-Weiss equation (Eqn. 1) in the whole temperature range, suggesting the occurrence of the dominance of weak antiferromagnetic interactions in the polycrystalline samples of these compounds (Θ = -1÷-2.6 K). The obtained magnetic parameters are listed in Table 4.

$$\chi_{para} = C/(T - \Theta) \qquad (1)$$

On the other hand, **1c** and **1e** showed essentially different temperature dependent magnetic behavior. Thus, $\chi_{para}T$ vs. *T* plots for **1c** can be fitted using Curie-Weiss equation (Eqn. 1) with a positive Weiss temperature (Θ = +0.33 K), suggesting the occurrence of dominance of weak ferromagnetic interactions in the temperature range of 3.7- 300 K. In the temperature below 3.7

K, a different type of intermolecular magnetic interactions with the negative sign starts prevailing. The crystalline state of **1e** showed significant antiferromagnetic interactions with a χ_{para} maximum at 32 K. The χ_{para} vs. T and $\chi_{para}T$ vs. T plots were well reproduced using the Bleany-Bowers equation (Eqn.2) (antiferromagnetic dimer model) with $J/\underline{k}_B$= -26 K taking into account the presence of the isolated radicals (0.6%) in the whole temperature range.

$$\chi_{para} = \frac{2N_A g^2 \beta^2}{3k_B T}\left[1 + \frac{1}{3}exp\left(-\frac{2J}{k_B T}\right)\right]^{-1} \quad (2)$$

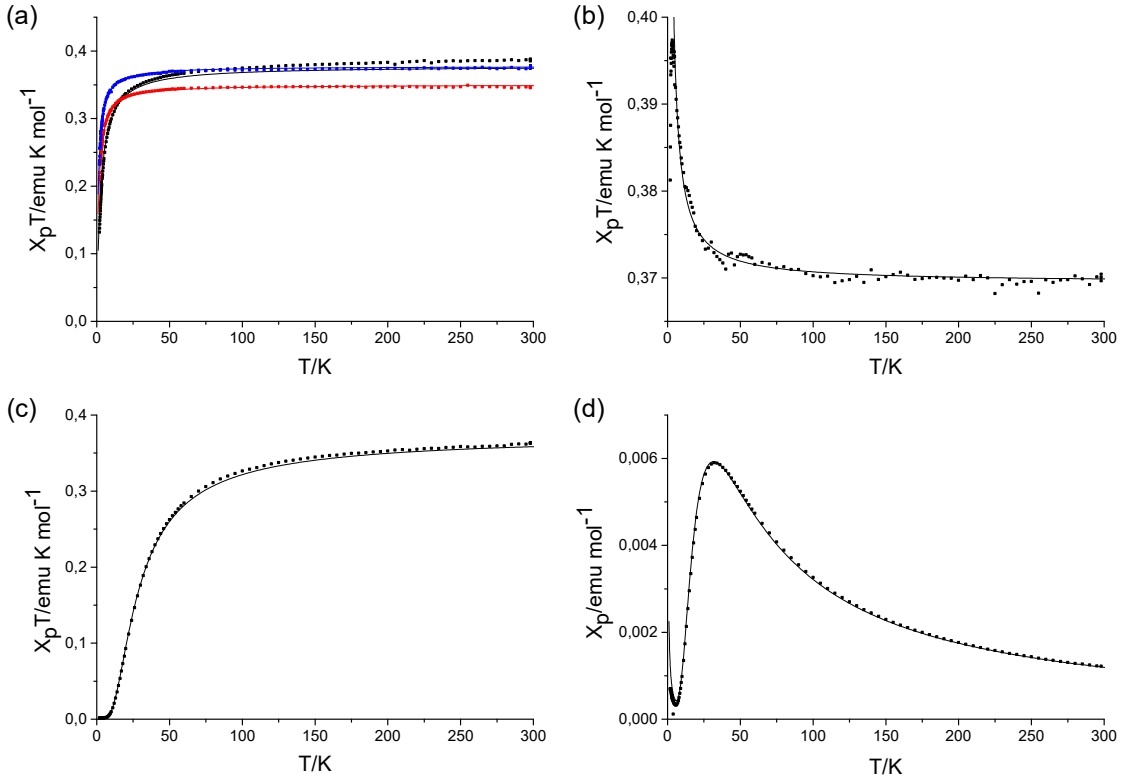

Figure 7. The SQUID magnetometry of the polycrystalline (solid) radicals **1a-e**: (a), (b) and (c) $\chi_{para}T$vs. T χ_{para} vs. T plots for (a) **1a** (black);, **1b** (red); **1d** (blue); (b) **1c**; (c) and (d) **1e**. The dotted curves denote the experimental values and the solid curves the calculated Curie-Weiss curves in (a),(b) or Bleany-Bowers curve (J/k_B = -25.6 K + Curie curve in (c) and (d).

Table 4. The magnetic parameters for **1a-e** obtained from the SQUID measurements

Compound	χ_{dia}/emu mol^{-1}	Purity/%	Curie constant/emu K mol^{-1}	Weiss Temperature/K	J/k_B/K
1a	-200×10^{-6}	100	0.378	-2.6	-
1b	-180×10^{-6}	92.8	0.350	-1.2	-
1c	-250×10^{-6}	97.9	0.370	+0.33	-
1d	-280×10^{-6}	100	0.377	-1.0	-
1e	-221×10^{-6}	98.8	–	-	-25.6

The observed magnetic behavior of **1a-e** can be explained on the basis of their crystal structures. In fact, the single crystal X-Ray diffraction analysis showed arrays of C-O(phenoxyl)...Me(nitroxide) (**1a**, **b**) or (N)O-C(arom) (**1c-e**) ferromagnetic 1D chains and inverse related C(phenoxyl)...Me(phenoxyl) or N(nitroxide)...Me(phenoxyl) antiferromagnetic dimers (**1c-e**) forming 3D networks throughout the lattices. Differences in the chemical structure of the hybrid radicals and, as a consequence, in the spatial arrangements and intermolecular interaction schemes lead to variations of the values of the corresponding intermolecular spin-spin exchange coupling parameters (J_{inter}), so as for ferromagnetic or antiferromagnetic coupling to emerge in the bulk magnetic properties. Since **1c** and **1e** showed the most interesting magnetic properties, we attempted to analyze their magneto-structural relationships precisely. Figure 8(a) and (b) represent head-over-tail dimers (indicated by red arrows) and 1D head-to-tail chains (indicated by blue arrows) in the single crystals of **1c** and**1e**, respectively. The corresponding contact distances, calculated Mulliken atomic spin populations and the values of J_{inter}'s for each considered pair of interacting radicals are summarized in Table 5 and Fig. 8. It can be seen from Fig. 8 that the **1e** dimers are much more symmetrical and contain more channels for the

intermolecular spin-spin exchange than in the case of the **1c** dimers. More specifically, the first **1e** dimer has two relatively close N(heteroarom)-C(Me) contacts and the second one contains C(heteroarom)-C(arom) contacts so that the contacted atoms possess sizable spin densities. The broken symmetry calculations for the dimers revealed that the exchange interactions in the first dimer are significantly stronger than in the second one (-25.24 K vs. -2.04 K) and are in good agreement with the experimentally obtained value (-25.6 K). In the case of **1c**, due to the symmetry breaking there are no contacts with considerable amounts of the values of the spin density on the interacting atoms. As a result, the corresponding spin-spin interactions are much weaker than in **1e** (-1.15 K as calculated). Referred to some significant difference between **1c** and **1e**, both of which form ferromagnetically weakly coupled infinity chains, the number of the corresponding contacts in the **1c** chains are greater than that in the **1e** chain, possibly giving difference in the macroscopic magnetic properties. The corresponding broken symmetry calculations correctly predict the sign of the spin-spin interactions, but their absolute values are underestimated.

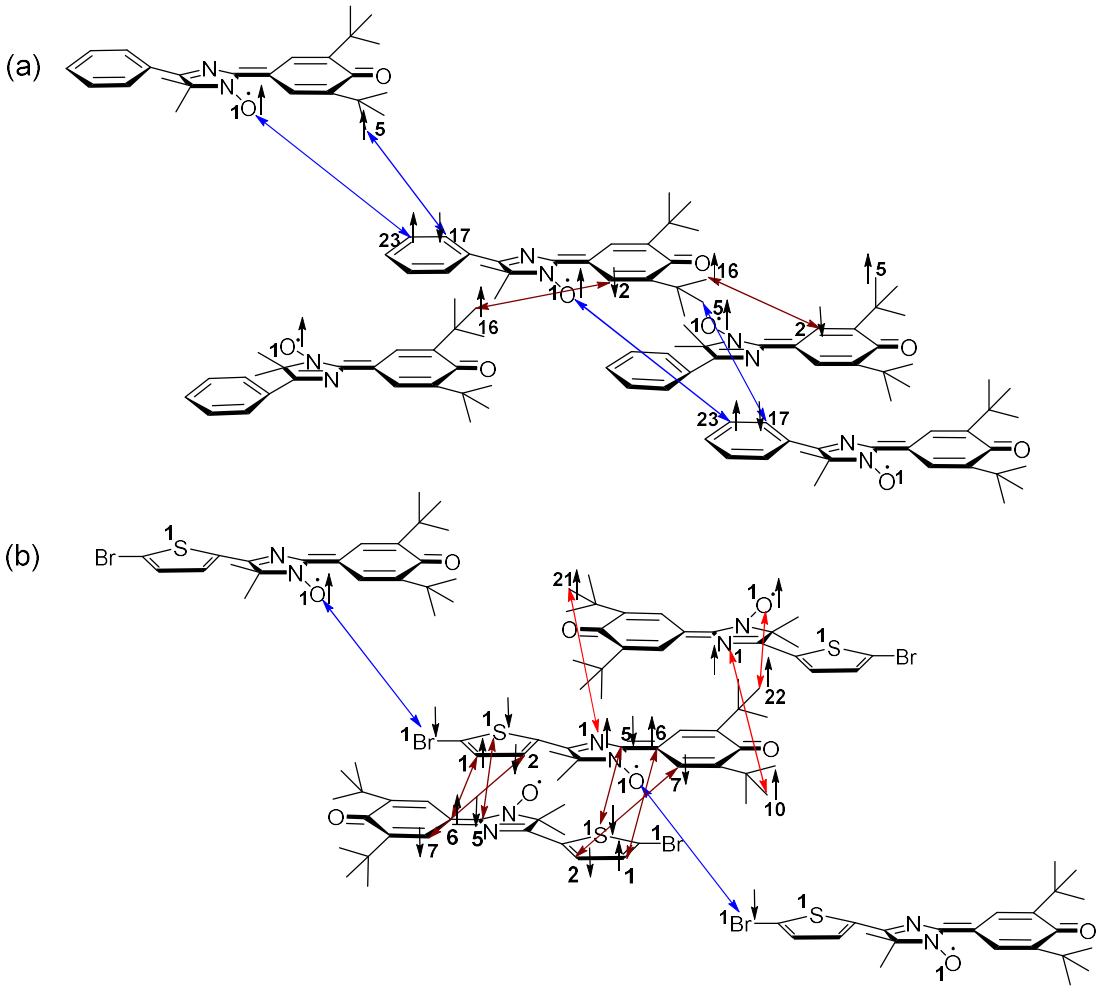

Figure 8. The short contacts in the single crystals of (a) **1c** and (b) **1e**. The blue arrows represent contacts in the ferromagnetic head-over-tail chains and the red ones -contacts in the antiferromagnetic head-to-tail dimers.

Table 5. The short contacts between the atoms with the significant absolute values of Mulliken atomic spin populations,*the corresponding distances and the calculated intermolecular spin-spin exchange interactions J_{inter}**in the single crystals of **1c** and **1e**.

Compound	Contacts between the labeled atoms and the corresponding Milliken atomic spin population*	Distance between the labeled atoms/Å	Calculated intermolecular spin-spin exchange interactions J/k_B/K*
1c			
Antiferromagnetic dimer	C2(-0.1135)-C16(0.0033)	3.478	-1.15
Ferromagnetic 1D chain	O1(0.3615)-C23(0.0105)	3.310	0.23
	C5(0.0068)-C17(-0.0199)	3.518	
1e			
Antiferromagnetic dimer 1	N1(0.0627)-C21(0.0057)	3.440	-25.24
	N1(0.0627)-H18(0.0007)	2.853	
Antiferromagnetic dimer 2	S1(-0.0042)-C5(-0.1736)	3.645	-2.04
	C1(0.0130)-C6(0.2727)	3.523	
	C2(-0.0376)-C7(-0.1066)	3.469	
Ferromagnetic 1D chain	O1(0.3704)-Br1(-0.0022)	2.809	3.18

*Mulliken atomic spin populations were calculated at the UB3LYP/cc-PVDZ level of theory.

**Broken symmetry DFT calculations were performed at the UB3LYP/def2-TZVP level of theory.

4. CONCLUSIONS

A series of the hybrid radicals, compactly hybridized phenoxyl nitroxides **1a-e** were synthesized and crystallized intended as useful building blocks in the quest for advanced molecular magnetism. Their salient feature is in the sizable π- spin delocalization extended to the phenoxyl moiety from the nitroxide moiety, and their electronic structures were thoroughly studied in terms of the spin density distributions and magnetic tensors. A significant difference from non-delocalized nitroxides has been identified in terms of contributions of the spin-orbit interaction enhanced via the extended π-conjugation to the phenoxyl group. We note that the theoretical **g**-

tensors and hyperfine coupling parameters are functional-dependent and the dependency is less for the **g**-tensors. In this context, among the functionals of B3LYP, BLYP, M06, B97-D, wB97XD, and BP86, importantly B97-D reproduces the experimental isotropic *g*-values and hyperfine coupling parameters for the spin delocalized hybrid radicals (SI). Thus, the functional B97-D seems a better choice for spin delocalized molecular systems to interpret the magnetic properties.

The hybrid phenoxyl-nitroxides **1a-e** revealed significant substituent effects on the macroscopic magnetic behavior due to both differences in the spin density distributions and molecular arrangements in their own crystals. The observed magnetic properties in the crystalline state were explained in terms of the molecular structural contact schemes which are based on the single-crystal X-ray diffraction data and the DFT calculations for the evaluation of intermolecular exchange interactions between the contacted radicals in the crystal lattice. The crystals were found to form the antiferromagnetic head-over-tail dimers and ferromagnetic head-to-tail chains, and as a result, depending on the hybrid radical and temperature, positive or negative exchange interactions dominate in the 3D crystal lattices. The findings suggest that hybrid nitroxides having a sizable amount of the extended π-spin delocalization are capable of building blocks for advanced molecular magnetic materials. Biradicals based on hybrid phenoxyl-nitroxides are designed and their syntheses are underway.

Supporting information. Synthetic procedures, analytical and spectroscopic data for hybrid radicals **1a-c,e** and intermediates; the calculated SOMO orbitals and spin density distributions for **1a-e**; functional dependence of the *g*-tensors and hyperfine coupling parameters for **1a-e**.

AUTHOR INFORMATION

Corresponding Authors

*E-mail: elena@nioch.nsc.ru. Phone: +73833309432

*E-mail:d-mazhukin@yandex.ru. Phone: +73833306852

*E-mail: sato@sci.osaka-cu.ac.jp. Phone:+81-6-6605-3072

*E-mail: takui@sci.osaka-cu.ac.jp. Phone:+81-6-66052605

Author Contributions

The manuscript was written through contributions of all authors. All authors have given approval to the final version of the manuscript.

ACKNOWLEDGMENT

The authors would like to thank Ministry of Education and Science of the Russian Federation (state contract no. 14. W03.31.0034), JSPS-RFBR Grant (17-53-50043). We are thankful to the Multi-Access Chemical Research Center SB RAS for spectral and analytical measurements. This work was also supported by Grants-in-Aid for Scientific Research B (17H03012), Scientific Research C (18K03465) and C (17K05840) from the MEXT, Japan. This work was also supported by the AOARD Scientific Project on ‘‘Molecular Spins for Quantum Technologies’’ (Grant FA2386-17-1-4040, 4041), USA.

REFERENCES

1. Lahti, P. M. Structure−Property Relationships for Metal-Free Organic Magnetic Materials. *Adv. Phys. Org. Chem.* **2011**, 45, 93−169.
2. *Stable Radicals: Fundamentals and Applied Aspects of Odd-Electron Compounds*; Hicks, R., Ed.; Wiley: New York, 2010.

3. Miller, J. S.; Drillon, M. In *Magnetism: Molecules to Materials IV*; Wiley-VCH: New York, 2003.
4. Tamura, M.; Nakazawa, Y.; Shiomi, D.; Nozawa, K.; Hosokoshi, Y.; Ishikawa, M.; Takahashi, M.; Kinoshita, M. Bulk Ferromagnetism in the Beta-Phase Crystal of the Para-Nitrophenyl Nitronyl Nitroxide Radical. *Chem. Phys. Lett.* **1991***, 186*, 401-404.
5. Allemand, P. M.; Khemani, K. C.; Koch, A.; Wudl, F.; Holczer, K.; Donovan, S.; Gruner, G.; Thompson, J. D. Organic Molecular Soft Ferromagnetism in a Fullerene C60. *Science* **1991**, *253*, 301-302.
6. Nakazawa, Y.; Tamura, M.; Shirakawa, N.; Shiomi, D.; Takahashi, M.; Kinoshita, M.; Ishikawa, M. Low-Temperature Magnetic Properties of the Ferromagnetic Organic Radical, Para-Nitrophenyl Nitronyl Nitroxide. *Phys. Rev. B* **1992**, *46*, 8906-8914.
7. Chiarelli, R.; Novak, M. A.; Rassat, A.; Tholence, J. L. A Ferromagnetic Transition at 1.48 K in an Organic Nitroxide. *Nature* **1993**, *363*, 147-149.
8. Sugawara, T.; Matsushita, M. M.; Izuoka, A.; Wada, N.; Takeda, N.; Ishikawa, M. An Organic Ferromagnet - Alpha-Phase Crystal of 2-(2',5'-Dihydroxyphenyl)-4,4,5,5-Tetramethyl-4,5-Dihydro-1H-Imidazolyl-1-Oxy-3-Oxide (Alpha-HQNN). *J. Chem. Soc., Chem. Commun.* **1994**, 1723-1724.
9. Matsushita, M. M.; Izuoka, A.; Sugawara, T.; Kobayashi, T.; Wada, N.; Takeda, N.; Ishikawa, M. Hydrogen-Bonded Organic Ferromagnet. *J. Am. Chem. Soc.* **1997**, *119*, 4369-4379.
10. Hosokoshi, Y.; Katoh, K.; Nakazawa, Y.; Nakano, H.; Inoue, K. Approach to a Single-Component Ferrimagnetism by Organic Radical Crystals. *J. Am. Chem. Soc.* **2001**, *123*, 7921-7922.
11. Shiomi, D.; Kanaya, T.; Sato, K.; Mito, M.; Takeda, K.; Takui, T. Single-Component Molecule-Based Ferrimagnetics. *J. Am. Chem. Soc.* **2001**, *123*, 11823-11824.
12. Fujita, W.; Awaga, K. Organic Ferromagnetism of T_c = 6.7 K Driven by Evaporation of Crystal Solvent. *Chem. Phys. Lett.* **2002**, *357*, 385-388.
13. Alberola, A.; Less, R. J.; Pask, C. M.; Rawson, J. M.; Palacio, F.; Oliete, P.; Paulsen, C.; Yamaguchi, A.; Farley, R. D.; Murphy, D. M. A Thiazyl-Based Organic Ferromagnet. *Angew. Chem., Int. Ed.* **2003**, *42*, 4782-4785.
14. Robertson, C. M.; Leitch, A. A.; Cvrkalj, K.; Reed, R. W.; Myles, D. J.; Dube, P. A.; Oakley, R. T. Enhanced Conductivity and Magnetic Ordering in Isostructural Heavy Atom Radicals. *J. Am. Chem. Soc.* **2008**, *130*, 8414-8425.
15. Shiomi, D.; Kanzaki, Y.; Okada, S.; Arima, R.; Miyazaki, Y.; Inaba, A.; Tanaka, R.; Sato, K.; Takui, T. An Enantiopair of Organic Ferromagnet Crystals Based on Helical Molecular Packing of Achiral Organic Radicals. *J. Phys. Chem. Lett.* **2011**, *2*, 3036-3039.
16. Rajca, A.; Takahashi, M.; Pink, M.; Spagnol, G.; Rajca, S. Conformationally Constrained, Stable, Triplet Ground State (S = 1) Nitroxide Diradicals. Antiferromagnetic Chains of S = 1 Diradicals. *J. Am. Chem. Soc.* **2007**, *129*, 10159-10170.
17. Rajca, A.; Shiraishi, K.; Rajca, S. Stable Diarylnitroxide Diradical with Triplet Ground State. *Chem. Commun.* **2009**, 4372-4374.
18. Suzuki, S.; Furui, T.; Kuratsu, M.; Kozaki, M.; Shiomi, D.; Sato, K.; Takui, T.; Okada, K. Nitroxide-Substituted Nitronyl Nitroxide and Iminonitroxide. *J. Am. Chem. Soc.* **2010**, *132*, 15908-15910.
19. Rajca, A.; Olankitwanit, A.; Rajca, S. Triplet Ground State Derivative of Aza-m-Xylylene Diradical with Large Singlet-Triplet Energy Gap. *J. Am. Chem. Soc.* **2011**, *133*, 4750-4753.

20. Kuratsu, M.; Suzuki, S.; Kozaki, M.; Shiomi, D.; Sato, K.; Takui, T.; Kanzawa, T.; Hosokoshi, Y.; Lan, X. Z.; Miyazaki, Y.; Inaba, A.; Okada, K. (Nitronyl Nitroxide)-Substituted Trioxytriphenylamine Radical Cation Tetrachlorogallate Salt: A 2p-Electron-Based Weak Ferromagnet Composed of a Triplet Diradical Cation. *Chem. - Asian J.* **2012**, *7*, 1604-1609.
21. Gallagher, N. M.; Bauer, J. J.; Pink, M.; Rajca, S.; Rajca, A. High-Spin Organic Diradical with Robust Stability. *J. Am. Chem. Soc.* **2016**, *138*, 9377-9380.
22. Amaya, N.; Ono, T.; Oku, Y.; Yamaguchi, H.; Matsuo, A.; Kindo, K.; Nojiri, H.; Palacio, F.; Campo, J.; Hosokoshi, Y. Spin-1/2 Quantum Antiferromagnet on a Three-Dimensional Honeycomb Lattice Formed by a New Organic Biradical F_4BIPBNN. *J. Phys. Soc. Jpn.* **2017**, *86*, 074706.
23. Yamaguchi, H.; Yoshizawa, D.; Kida, T.; Hagiwara, M.; Matsuo, A.; Kono, Y.; Sakakibara, T.; Tamekuni, Y.; Miyagai, H.; Hosokoshi, Y. Magnetic-Field-Induced Quantum Phase in S = 1/2 Frustrated Trellis Lattice. *J. Phys. Soc. Jpn.* **2018**, *87*, 043701.
24. Kanetomo, T.; Ichihashi, K.; Enomoto, M.; Ishida, T. Ground Triplet Spirobiradical: 2,2',7,7'-Tetra(tert-butyl)-9,9'(10H,10'H)-Spirobiacridine-10,10'-Dioxyl. *Org. Lett.* **2019**, *21*, 3909-3912.
25. Gallagher, N.; Zhang, H.; Junghoefer, T.; Giangrisostomi, E.; Ovsyannikov, R.; Pink, M.; Rajca, S.; Casu, M. B.; Rajca, A. Thermally and Magnetically Robust Triplet Ground State Diradical. *J. Am. Chem. Soc.* **2019**, *141*, 4764-4774.
26. Winter, S. M.; Balo, A. R.; Roberts, R. J.; Lekin, K.; Assoud, A.; Dube, P. A.; Oakley, R. T. Hybrid Dithiazolothiadiazinyl Radicals; Versatile Building Blocks for Magnetic and Conductive Materials. *Chem. Commun.* **2013**, *49*, 1603-1605.
27. Yu, X.; Mailman, A.; Dube, P. A.; Assoud, A.; Oakley, R. T. The First Semiquinone-Bridged Bisdithiazolyl Radical Conductor: A Canted Antiferromagnet Displaying a Spin-Flop Transition. *Chem. Commun.* **2011**, *47*, 4655-4657.
28. Vasko, P.; Hurmalainen, J.; Mansikkamaki, A.; Peuronen, A.; Mailman, A.; Tuononen, H. M. Synthesis of New Hybrid 1,4-Thiazinyl-1,2,3-Dithiazolyl Radicals via Smiles Rearrangement. *Dalton Trans.* **2017**, *46*, 16004-16008.
29. Decken, A.; Mailman, A.; Passmore, J.; Rautiainen, J. M.; Scherer, W.; Scheidt, E. W. A Prototype Hybrid 7π Quinone-Fused 1,3,2-Dithiazolyl Radical. *Dalton Trans.* **2011**, *40*, 868-879.
30. Bonanno, N. M.; Poddutoori, P. K.; Sato, K.; Sugisaki, K.; Takui, T.; Lough, A. J.; Lemaire, M. T. Reversible Solution pi-Dimerization and Long Multicenter Bonding in a Stable Phenoxyl Radical. *Chem. - Eur. J.* **2018**, *24*, 14906-14910.
31. Xie, C.; Lahti, P. M.; George, C. Modulating Spin Delocalization in Phenoxyl Radicals Conjugated with Heterocycles. *Org. Lett.* **2000**, *2*, 3417-3420.
32. Taylor, P.; Lahti, P. M. Crystallography and Magnetism of Radicals with Hindered Hydroxyl Groups: 2-(3,5-Di-tert-Butyl-4-Hydroxyphenyl)-4,4,5,5-Tetramethyl-4,5-Dihydro-1H-Imidazole-3-Oxide-1-Oxyl and 2-(3,5-Di-tert-Butyl-4-Hydroxyphenyl)-4,4,5,5-Tetramethyl-4,5-Dihydro-1H-Imidazole-1-Oxyl. *Chem. Commun.* **2004**, 2686-2688.
33. Ten, Y. A.; Salnikov, O. G.; Amitina, S. A.; Stass, D. V.; Rybalova, T. V.; Kazantsev, M. S.; Bogomyakov, A. S.; Mostovich, E. A.; Mazhukin, D. G. The Suzuki-Miyaura Reaction as a Tool for Modification of Phenoxyl-Nitroxyl Radicals of the 4H-Imidazole N-Oxide Series. *RSC Adv.* **2018**, *8*, 26099-26107.
34. Frisch, M. J.; Trucks, G. W.; Schlegel, H. B.; Scuseria, G. E.; Robb, M. A.; Cheeseman, J. R.; Scalmani, G.; Barone, V.; Mennucci, B.; Petersson, G. A.; et al. *Gaussian 09,* Revision A.02; Gaussian: Wallingford, CT, USA, 2009.

35. Neese, F. The ORCA Program System. *Wiley Inderdiscip. Rev. Comput. Mol. Sci.* **2012**, *2*, 73-78.
36. Itoh, K.; Takui, T. High Spin Chemistry Underlying Organic Molecular Magnetism - Topological Symmetry Rule as The First Principle of Spin Alignment in Organic Open-Shell Systems of pi-Conjugation and Their Ions. *Proc. Jpn. Acad., Ser. B* **2004**, *80*, 29-40.
37. Likhtenshtein, G. I.; Yamauchi, J.; Nakatsuji, S.; Smirnov, A. I.; Tamura, R. In *Nitroxides: Applications in Chemistry, Biomedicine, and Materials Science*. Wiley-VCH: Weinheim, 2008.
38. Bally, T.; Borden, W. T., Calculations on Open-Shell Molecules: A Beginner's Guide. In *Rev. Comput. Chem.*, Lipkowitz, K. B.; Boyd, D. B., Eds. Wiley-VCH: 1999; Vol. 13, pp 1-97.

Proposed Picture for TOC